The International Journal of Advanced Manufacturing Technology (2018) 95:3905–3918
https://doi.org/10.1007/s00170-017-1494-4

ORIGINAL ARTICLE

Rigid-flexible coupling forming process for aluminum alloy automobile body panels

Yao Wang[1] · Lihui Lang[1] · Ehsan Sherkatghanad[1] · Karl Brian Nielsen[2] · Xiao Xing Li[1] · Zhi Ying Sun[1]

Received: 5 April 2017 / Accepted: 17 December 2017 / Published online: 2 January 2018

Abstract
A newly proposed method for the manufacturing of complex aluminum alloy automobile body panels is the rigid-flexible coupling forming process. The principle of this method is introduced and the key process parameters such as the hydraulic pressure loading path and rigid-flexible effect, blank holder force (BHF), and the draw bead setting are investigated by using numerical simulation and experiment. The relationship between the local rounded corner feature and the hydraulic pressure is theoretically analyzed specifically for the aluminum alloy inner panel of automobile engine hood. Meanwhile, the formability of this part is also surveyed in different parameters of the rigid-flexible coupling process. Finally, the applicability of the proposed method is validated by the results of experiments. The research exhibited that the rigid-flexible coupling forming process can be well used for manufacturing this kind of complex multi-feature sheet parts.

Keywords Lightweight · Rigid-flexible coupling · Aluminum alloy · Automobile body panel · Combined forming process

1 Introduction

With the rapid development of society and the constant progress of technology, the sustainable development has increasingly become one of the areas of interest. More and more people are paying attention to the limited resources and ever-increasing environmental pollution which bring serious damage to the health of human beings [1]. In the automobile manufacturing field, always the techniques of lightweight forming are utilized as the effective approaches to solve these problems. Adopting the lightweight materials to substitute the traditional steel materials such as aluminum alloy, magnesium alloy, and composite materials is essential to reach the purpose of weight loss. Meanwhile, the application of green flexible forming technique can solve the hard precision forming and poor surface quality problems of lightweight alloy materials effectively [2–4].

✉ Lihui Lang
langlh425@163.com

[1] School of Mechanical Engineering and Automation, Beihang University, No. 37 Xueyuan Road, Beijing 100191, China

[2] Department of Materials and Production, Aalborg University, Fibigerstraede16, Aalborg DK-9220, Denmark

Nowadays, the chosen materials for the automobile body panel are mainly 5xxx and 6xxx aluminum alloy series. Even though these kinds of materials have the advantages of high strength and better performance, the problems of low elongation at room temperature, poor plastic deformability, and severe spring back make the conventional stamping process difficult to meet the requirements of production. Furthermore, the rigid stamping is prone to cause scratch at the surface of the aluminum sheet and easily produce defects in the impact line and slip line, which are hard to meet the demands of high accuracy in the automobile panel surface [5, 6]. In order to deal with the manufacturing difficulties of the aluminum body panel, some advanced forming processes continuously appear, such as hot stamping, superplastic forming, viscous medium pressure forming, and so on. These technologies are effectively used to form aluminum alloy materials. However, due to the cost and the efficiency, it is difficult to realize the mass production of panel parts [7–9]. In fact, the hydroforming technology uses the fluid to assist forming. During the forming process, the blank is tightly pressed on the punch and the beneficial friction is built under the hydraulic pressure, avoiding the excessive thinning or even fracture at the deformation danger zone (around the small rounded corner). Meanwhile, the fluid spills on to the area between the lower surface of the blank and the upper surface of the die to make the fluid lubrication. Therefore, the friction force between the aluminum alloy material and the rigid tools is

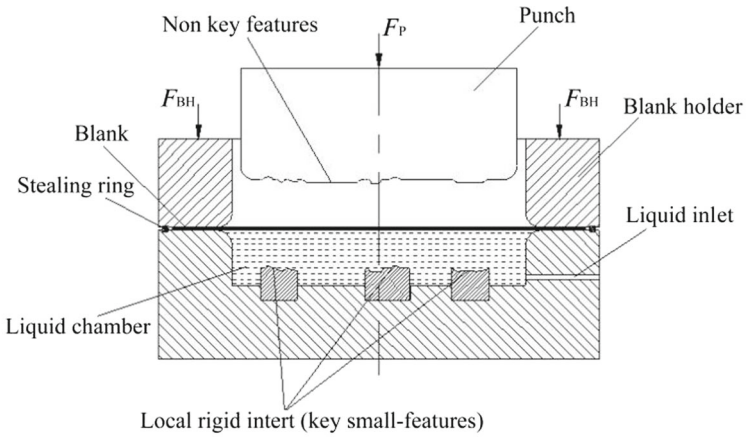

(a) Schematic diagram of process principle

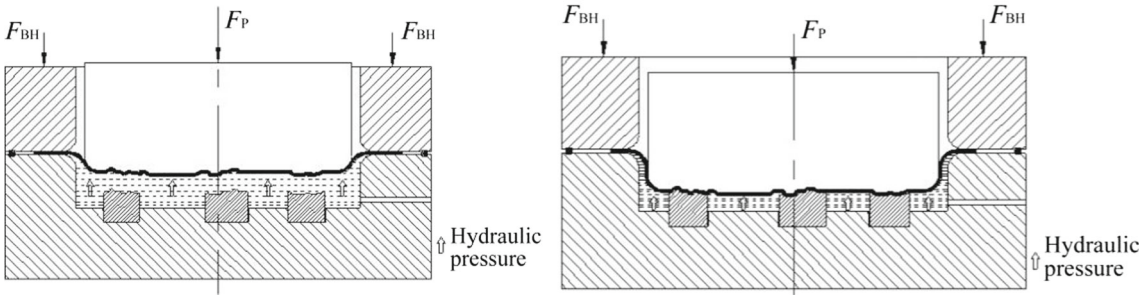

(b) Schematic diagram of hydroforming stage (c) Schematic diagram of rigid-flexible coupling stage

Fig. 1 Schematic diagram of the proposed forming process. **a** Schematic diagram of process principle. **b** Schematic diagram of hydroforming stage. **c** Schematic diagram of rigid-flexible coupling stage

reduced, which is beneficial for the material to flow into the die cavity. The hydroforming process can be used widely for the precision forming of large aluminum alloy panel parts without heating in automobile industries, the

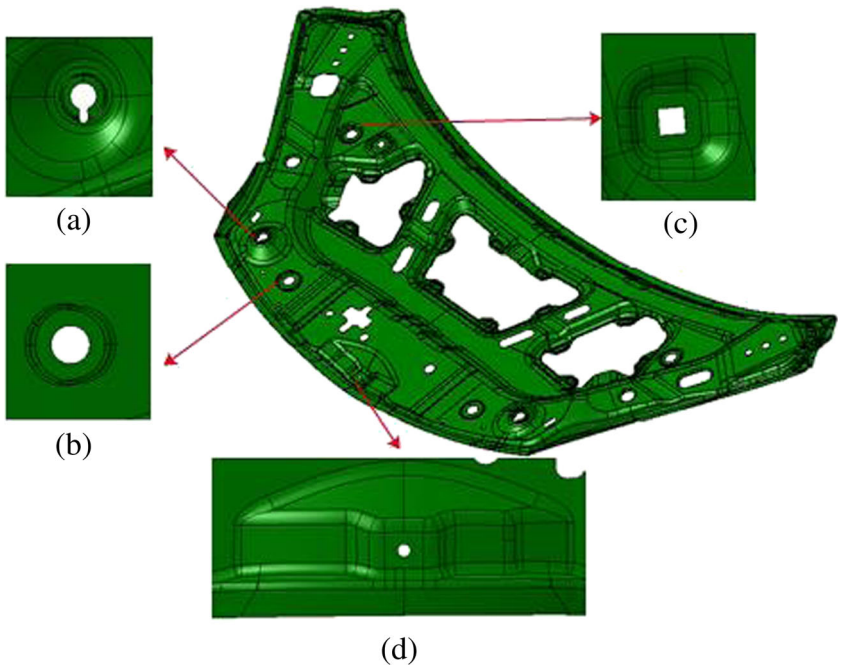

Fig. 2 Overall dimensions and key local features of the part

Table 1 Mechanical properties of 5182-O sheet metal

Angle with rolling direction	Yield strength (MPa)	Tensile strength (MPa)	Strain hardening	Anisotropy coefficient
0°	119	271	0.34	0.73
45°	118	266	0.34	0.65
90°	116	264	0.34	0.60

production efficiency and the surface quality of the forming parts are superior [10–12].

There are a few research reports about the production of automobile aluminum alloy panel part adopting the hydroforming technology. The American General Motors (GM) [13] has developed mass production of car-Corvette Z06 using the aluminum alloy hydroforming. Schuler Company [14] employed pre-bulging hydro-mechanical deep drawing technology to form the aluminum alloy roof panel with the size of 2200 mm × 1600 mm × 200 mm and the thickness of 1.0 mm. The results demonstrated that the pre-bulging can increase the denting-resistance of the part (about 7%) and the thinning ratio of the center point (from 2 to 5%). The external surface quality of the part is grade 2, which is superior to that of the common stamping. Amino North America Company [15] utilized the hydro-mechanical deep drawing technique to develop the aluminum alloy automobile body panel parts such as the inner and outer panel of the engine hood, the door panel, and the front fender. Palumbo [16] investigated the possibility of manufacturing a small-sized car door panel using the sheet hydroforming process and rapid tooling technique. The proposed approach was proved to be effective in rapidly manufacturing prototypes and thus in shortening the product design process. Liu et al. [17] studied on the hydro-mechanical deep drawing and the variable blank holder force technologies of the AA6009 outer panel of the door. The matching relationship between the hydraulic pressure loading path and the blank holder force was optimized, and the specimen was obtained with a high forming precision and a uniform wall thickness distribution.

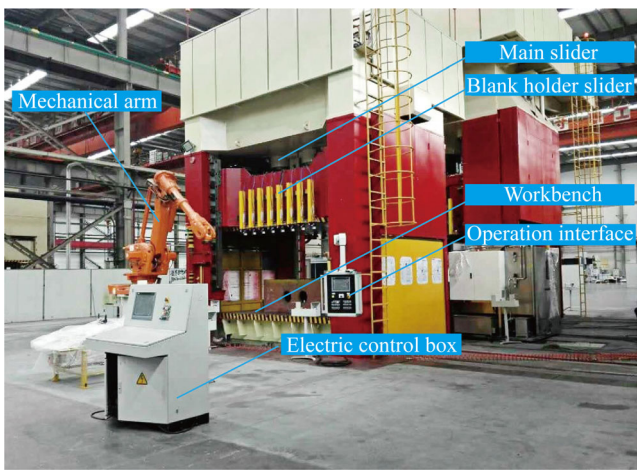

Fig. 3 The 50,000 kN sheet hydroforming equipment

A lot of researches have shown that the hydroforming technology is difficult to accurately form the small rounded corner/small-feature of the part, resulting in the high hydraulic pressure, equipment tonnage, and cost. Based on this fact, the rigid-flexible coupling forming process is proposed in this paper, combing the hydroforming and rigid forming in a single stage and having both forming advantages. It provides a new way for hydroforming the sheet metal parts with small-features and multi-features and broadens the complexity and functional requirement of the parts formed by hydroforming. Meanwhile, the principle and key process parameters of this process are analyzed, which will offer the academic and theoretical foundation for the further research and application of the new process.

In this paper, the relationship between the local rounded corner feature and the hydraulic pressure is theoretically analyzed specifically for the aluminum alloy inner panel of automobile engine hood. The formability of this part is surveyed in different parameters of the rigid-flexible coupling process. Meanwhile, the applicability of the proposed process is validated by the results of experiments.

2 Rigid-flexible coupling forming process

The rigid-flexible coupling forming process is a new derivative technique combing the hydroforming and rigid forming in a single stage, having both forming advantages. The process contains the rapid rehydration and then the sheet blank is put on the surface of the liquid chamber flange and clamped by descending the blank holder. Then, the punch goes down and the blank is touched. It continues to go down at a certain speed, and at the same time the chamber is filling to pressurize. The blank is pushed into the liquid chamber and generate elastic-plastic deformation under the synthetic effect of the punch and hydraulic pressure. The most of the features are formed, but the small local features and super small rounded corners are only formed partly in the process of going down. The precision shaping is realized between the punch and local rigid insert block, which is set up in the bottom of the liquid chamber, when they go down to a certain depth. The features that cannot be formed in the usual hydroforming stage are further formed and the rigid-flexible coupling process is achieved. The schematic diagram of forming process is showed in Fig. 1.

(a) The punch (b) Local rigid insert block (die)

Fig. 4 The tools. **a** The punch. **b** Local rigid insert block (die)

After finishing the first installation, the tools used in the process can meet all the process requirements of forming and shaping, guaranteeing the whole required precision of the product. In addition, the use of local rigid mold can greatly reduce the needed equipment tonnage of hydroforming. And the mold debugging time is decreased and the production efficiency is increased. The local rigid mold can use in the form of insert block, which can be replaced at any time, increasing the flexibility of the mold. Meanwhile, this makes it easy to repair the mold for subsequent process, increasing the efficiency of repairing mold. The combined forming process has better forming result and quality for the hard-forming lightweight alloy materials and the complex components with a variety of small-feature sizes, such as the automobile inner panels. It would also broaden the complexity and functional requirement of the parts formed by hydroforming.

3 Experimental and numerical simulation condition

3.1 Part and used material

In this paper, the complex inner panel of the engine hood is developed by using rigid-flexible coupling forming process. Its overall dimensions and the key local features are shown in Fig. 2. The size is 1378.41 mm × 481.71 mm × 81.05 mm. The model characteristics are as follows: large overall size, a lot of local small features, and complex shapes including the minimum rounded corner radius of 2.0 mm. The figure shows four key local feature positions as the remained position of the rigid-flexible coupling die. The aluminum alloy 5182-O with the thickness of 1.0 mm was used and its mechanical properties obtained through uniaxial tensile test are shown in Table 1. As seen in the table, compared with the ordinary deep-drawing steel sheet, the formability of the aluminum alloy sheet is poor, which will bring the great difficulty for the manufacturing.

3.2 Test equipment and tooling

The 50,000 kN sheet hydroforming equipment is shown in Fig. 3. The equipment mainly consists of the host system, the high-pressure source system, the quick mold-change mechanism, and the integrated control system. The maximum hydraulic pressure can reach 60 MPa with control precision of ± 0.5 MPa. The nominal pressures of the main cylinder and blank holder cylinder are 35,000 and 15,000 kN, respectively. The size of the working table is 4500 mm × 3000 mm. Meanwhile, the equipment has independent electrical control box and bench board, which employ PLC controlling and can achieve centralized operation of all functional buttons. The tools and the form of the curved surface used for the blank holder surface are shown in Fig. 4. Under the hydraulic pressure, the blank deforms firstly to fit the punch, so the punch retains the whole features of the part entirely. The die consists

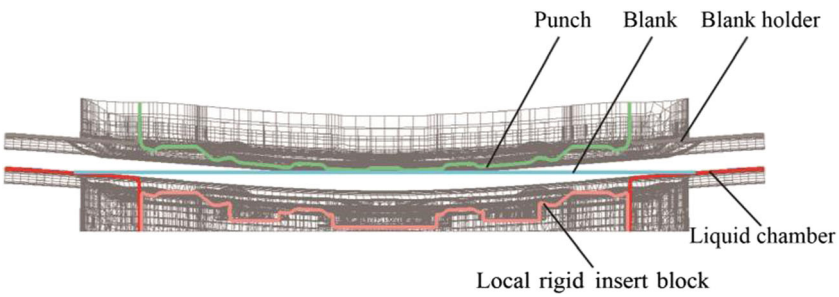

Fig. 5 Finite element model

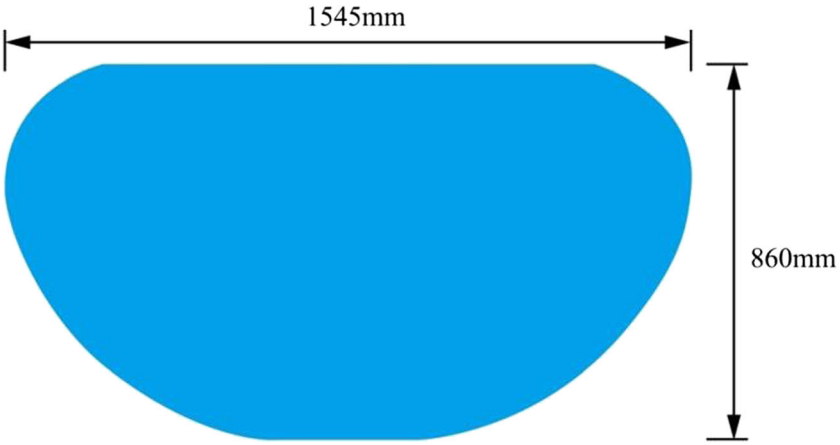

Fig. 6 Optimized blank shape

of the liquid chamber and local rigid insert block, achieving the rigid-flexible coupling forming eventually.

3.3 Numerical simulation condition

The commercial finite element software eta/Dynaform 5.8.1 was used for the numerical simulation of the rigid-flexible coupling forming process for the inner panel of the engine hood. The finite element model is shown in Fig. 5. The blank was discrete using the B-T shell element, and the tools were modeled using the rigid shell element. In order to describe the features of small rounded corners accurately, there should be at least 4 units on each corner, so the maximum mesh size is set to 10.0 mm and the minimum one is 0.1 mm with the calculation process of mesh refinement. Because of the friction conservation effect in the hydroforming, the friction coefficient of 0.17 was chosen for the interface between the blank and the punch [18]. Meanwhile, due to the fluid lubrication effect, the friction coefficient of 0.12 was chosen for the interfaces between the blank and the chamber and binder [19]. The optimized blank shape designed by combining the CAD modeling and the blank size estimate in CAE analysis is shown in Fig. 6.

4 Theoretical relationship between local rounded corner features and hydraulic pressure

In the process of rigid-flexible coupling forming of sheet metal, the hydraulic pressure loading path in the early stage has an important influence on the rigid-flexible effect and the final forming quality of the part. However, the size of the rounded corner feature is the key factor for designing the hydraulic pressure. In this section, the relationship between the local rounded corner features and the hydraulic pressure is given by theoretical calculation, which provides the theoretical basis for the design of the hydraulic pressure loading path.

Two kinds of rounded corners are formed and extracted from the specimen, named the convex and concave rounded corner, as shown in Fig. 7. For the forming of convex rounded corners, the blank is bent at the punch surface along the convex rounded corner under the action of the hydraulic pressure. The forming process is a complex process of plastic deformation. For its mechanical analysis, we need to do the corresponding simplified treatment. In the analysis, it is considered that the material at the convex rounded corner is pure bending. Meanwhile, the friction between the blank and the punch is neglected because the initial hydraulic pressure is low.

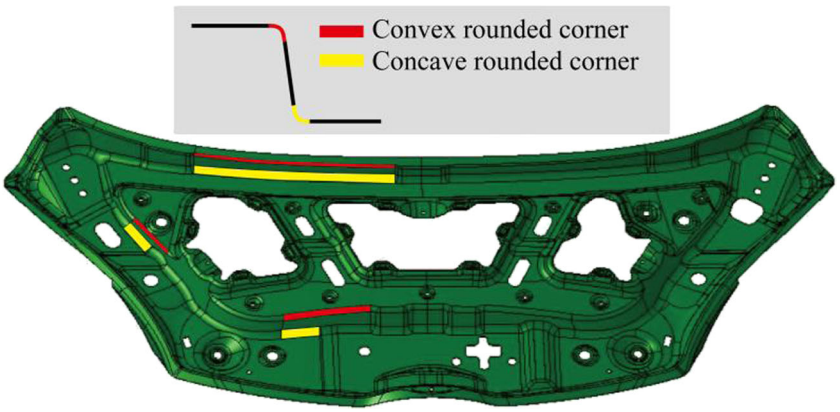

Fig. 7 Convex and concave rounded corner features

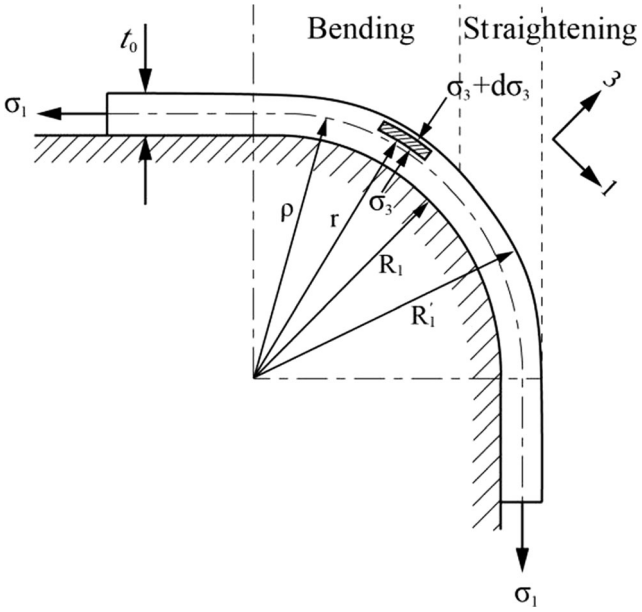

Fig. 8 Bending process of the convex rounded corner

If the neutral layer taking as the boundary, the outside is the tensile stress region and the inside is the compressive stress region. The plastic equation, the plane strain condition, and the differential equilibrium equation of these two regions can be expressed as [20]:

For the outside region (+):

$$\sigma_1+\sigma_3=\frac{1+\xi}{\sqrt{1+2\xi}}\sigma_s \tag{1}$$

$$\sigma_2=\frac{\xi\sigma_1-\sigma_3}{1+\xi} \tag{2}$$

$$d\sigma_3=-(\sigma_1+\sigma_3)\frac{dr}{r} \tag{3}$$

For the inside region (−):

$$\sigma_1-\sigma_3=\frac{1+\xi}{\sqrt{1+2\xi}}\sigma_s \tag{4}$$

$$\sigma_2=\frac{\xi\sigma_1+\sigma_3}{1+\xi} \tag{5}$$

$$d\sigma_3=(\sigma_1-\sigma_3)\frac{dr}{r} \tag{6}$$

where σ_1 is the tangential stress, σ_2 is the radial stress, and σ_3 is the transverse stress. σ_s is the yield strength. ξ is the normal anisotropy index.

The boundary conditions (as shown in Fig. 8):

$$r=R_1',\ \sigma_3=-p.\ r=R_1,\ \sigma_3=\sigma_c. \tag{7}$$

The normal stress σ_3 is continuous in the direction of thickness, so:

$$r=\rho,\ \sigma_3^+=\sigma_3^- \tag{8}$$

$$\rho=\sqrt{R_1R_1'} \tag{9}$$

The contact stress can be obtained as follows [21]:

$$\sigma_c=\frac{1+\xi}{\sqrt{1+2\xi}}\sigma_s\ln\sqrt{R_1R_1'}-p \tag{10}$$

where p is the hydraulic pressure.

The three principal stresses of the outside region (+) are as follows:

$$\sigma_1=\frac{1+\xi}{\sqrt{1+2\xi}}\sigma_s\left(1-\ln{R_1'}/{r}\right)+p \tag{11}$$

$$\sigma_2=\frac{1}{\sqrt{1+2\xi}}\sigma_s\left[\xi-(1+\xi)\ln{R_1'}/{r}\right]+p \tag{12}$$

$$\sigma_3=\frac{1+\xi}{\sqrt{1+2\xi}}\sigma_s\ln{R_1'}/{r}-p \tag{13}$$

The three principal stresses of the inside region (−) are as follows:

$$\sigma_1=\frac{1+\xi}{\sqrt{1+2\xi}}\sigma_s\left(1+\ln{r}/{R_1}\right)-p \tag{14}$$

$$\sigma_2=\frac{1}{\sqrt{1+2\xi}}\sigma_s\left[\xi+(1+\xi)\ln{r}/{R_1}\right]-p \tag{15}$$

$$\sigma_3=\frac{1+\xi}{\sqrt{1+2\xi}}\sigma_s\ln{r}/{R_1}-p \tag{16}$$

The average tangential stress can be expressed as [22]:

$$\sigma_1=\frac{\int_{\rho}^{R_1'}\sigma_1^+dr+\int_{R_1}^{\rho}\sigma_1^-dr}{t_0}=\frac{1+\xi}{\sqrt{1+2\xi}}\sigma_s\left({R_1'}/{t_0}\ln R_1'-{R_1}/{t_0}\ln R_1-\ln\sqrt{R_1R_1'}\right) \tag{17}$$

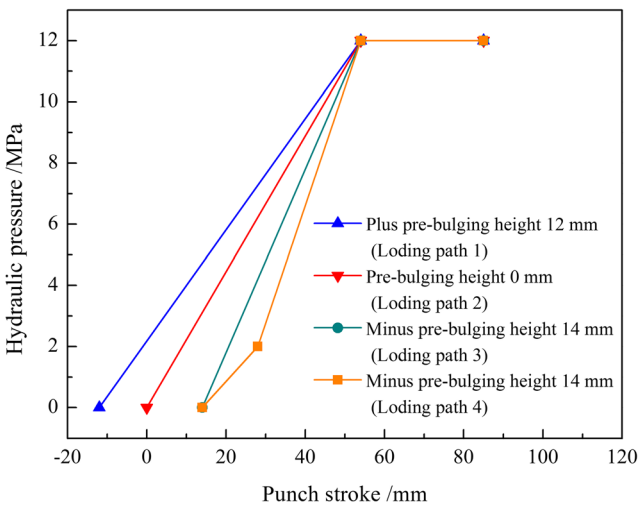

Fig. 9 Loading paths with different pre-bulging heights

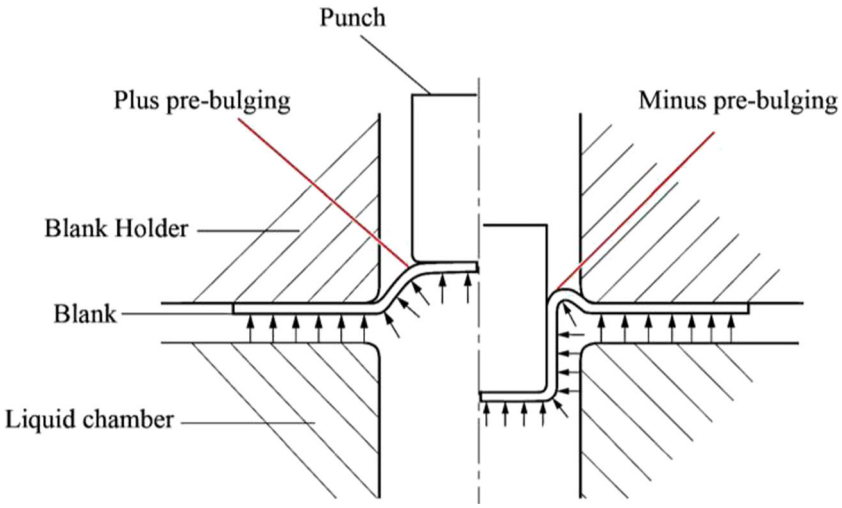

Fig. 10 Different pre-bulging methods: plus pre-bulging and minus pre-bulging

The incidental stress caused by bending and straightening deformations is as follows:

$$\Delta\sigma_1 = \frac{\sigma_b t_0}{2R_1 + t_0} \tag{18}$$

where σ_b is the tensile strength. Meanwhile, $\sigma_3 = -p$

So, the maximum equivalent stress of bending region of the convex rounded corner can be calculated by the following formula:

$$\overline{\sigma} = \frac{\sqrt{3}}{2}\left[\frac{1+\xi}{\sqrt{1+2\xi}}\sigma_s\left(R_1'\Big/_{t_0}\ln R_1' - R_1\Big/_{t_0}\ln R_1 - \ln\sqrt{R_1 R_1'}\right) + \frac{\sigma_b t_0}{2R_1 + t_0} + p\right] \tag{19}$$

In sheet tensile test, the true strain at fracture can be expressed as:

$$\varepsilon_f = -\ln(1-\lambda) \tag{20}$$

$$\lambda = \frac{A_0 - A_f}{A_0} \tag{21}$$

where λ is the fracture section reduction rate, A_0 is the initial cross section area at the fracture location, and A_f is the final cross section area at the fracture location.

The constitutive equation of the material is assumed to be as follows:

$$\sigma = K\varepsilon^n \tag{22}$$

So:

$$\sigma_f = K\varepsilon_f^n = -K\ln^n(1-\lambda) \tag{23}$$

The fracture condition of the convex rounded corner can be expressed as:

$$\overline{\sigma} = \sigma_f \tag{24}$$

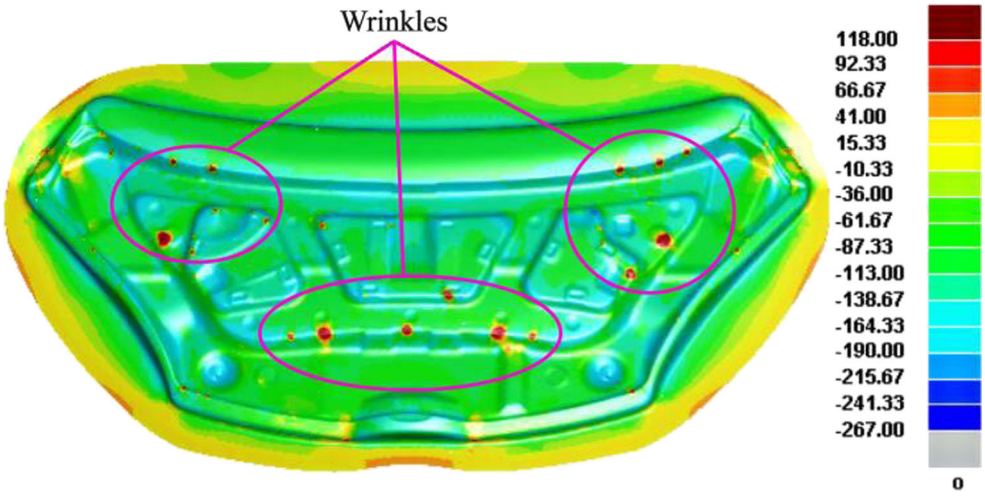

Fig. 11 Specimen multiple wrinkles or even fracture

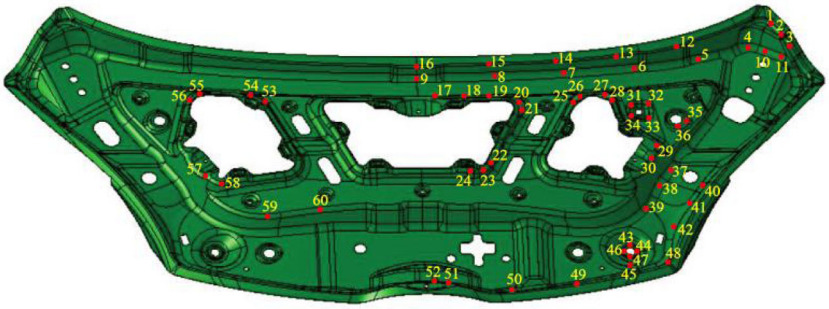

(a) Measuring point position

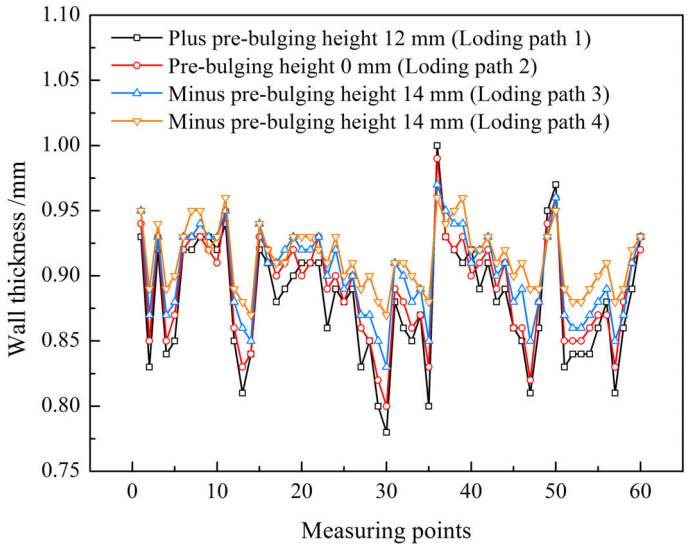

(b) Wall thickness distributions

Fig. 12 Wall thickness distributions of the specimen under the four kinds of loading paths. **a** Measuring point position. **b** Wall thickness distributions

The relation between the hydraulic pressure and the minimum relative radius of the convex rounded corner is obtained as follows:

$$p = \frac{2\sqrt{3}}{3} K \ln^n(1-\lambda) + \frac{1+\xi}{\sqrt{1+2\xi}}\sigma_s + \frac{(1+\xi)\sigma_s}{2r_1\sqrt{1+2\xi}} + \frac{2\sigma_b}{2r_1+1} \tag{25}$$

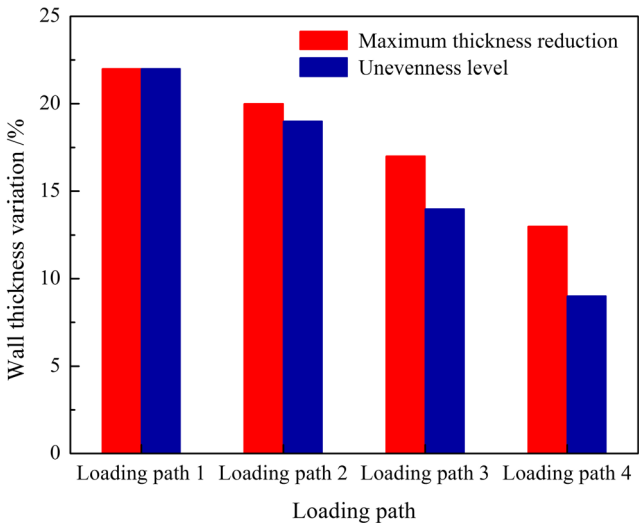

Fig. 13 Effects of pre-bulging on the maximum thickness reduction and unevenness level of wall thickness

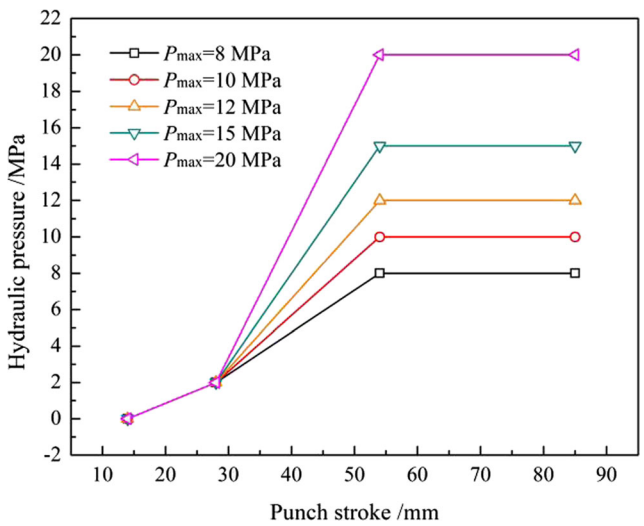

Fig. 14 Loading paths with different maximum hydraulic pressures

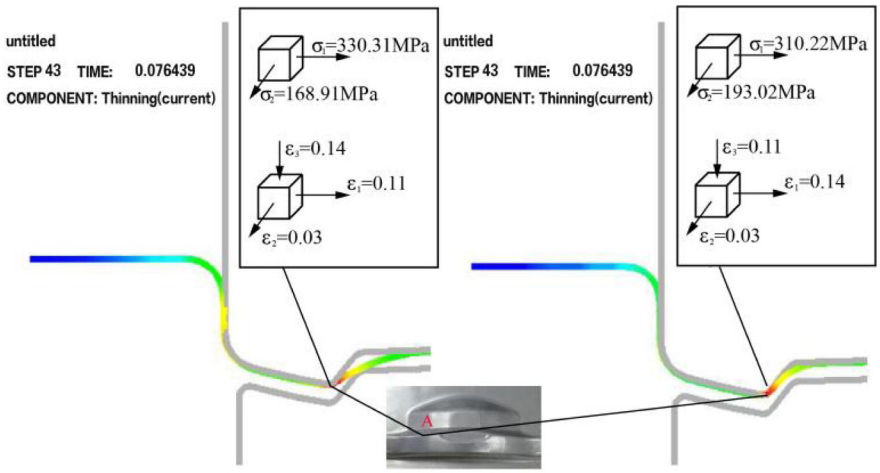

(a) Maximum hydraulic pressure of 8 MPa (left) and 20 MPa (right) at position A

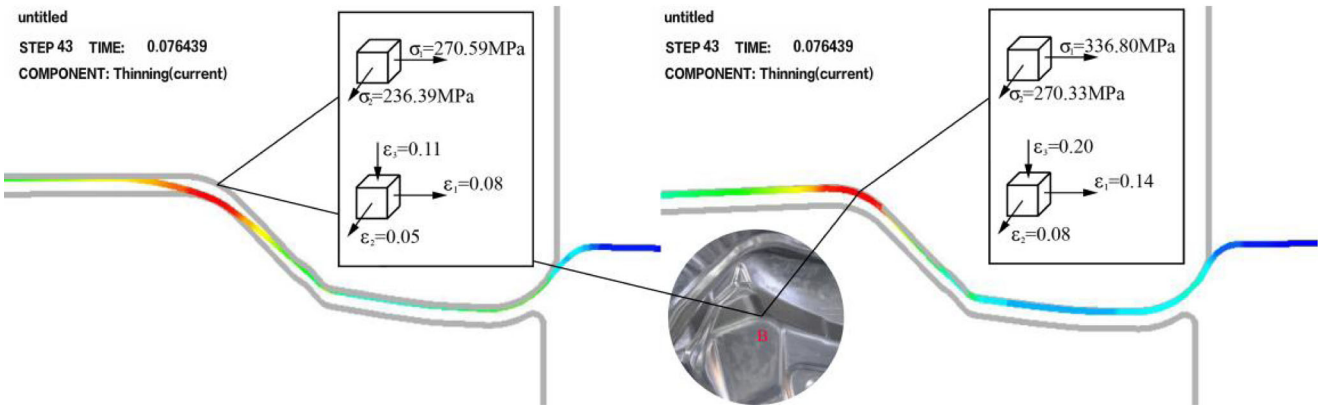

(b) Maximum hydraulic pressure of 8 MPa (left) and 20 MPa (right) at position B

Fig. 15 Punch fitting processes of the typical position A and B under different hydraulic pressure conditions. **a** Maximum hydraulic pressure of 8 MPa (left) and 20 MPa (right) at position A. **b** Maximum hydraulic pressure of 8 MPa (left) and 20 MPa (right) at position B

The relationship between the hydraulic pressure and the relative radius of the concave rounded corner can be expressed by the following formula:

$$p = \frac{\sigma_s + \sigma_b}{2r_2} \tag{26}$$

From the Eqs. (25) and (26) can be seen that the smaller convex and concave rounded corner radii, the greater hydraulic pressure required for forming process.

Fig. 16 Fracture at position A caused by hydraulic pressure 8 MPa

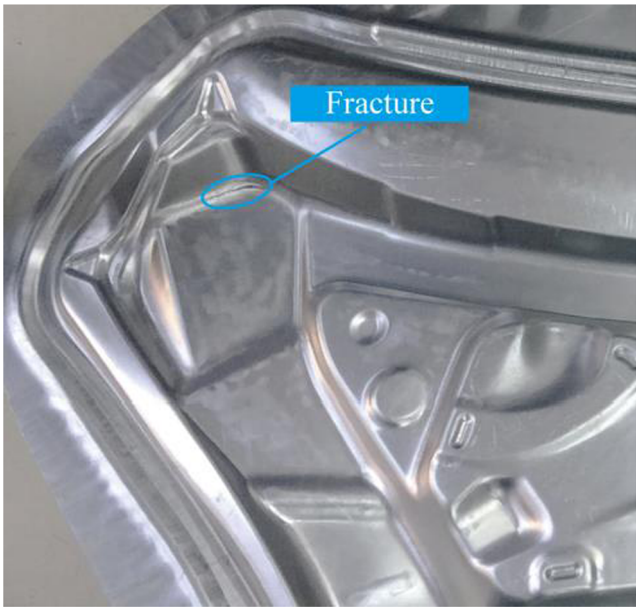

Fig. 17 Fracture at position B caused by hydraulic pressure 20 MPa

5 Analysis and discussion

5.1 Influences of hydraulic pressure loading path and rigid-flexible effect on the forming quality of inner panel

At the beginning of the forming process, the blank produces elastic-plastic deformation under the assisted action of hydraulic pressure, which will conduct the hydro-mechanical deep drawing. The pre-bulging effect is applied to perform at the initial stage (as shown in Fig. 9). According to the different position of the punch during pre-bulging forming process, as illustrated in Fig. 10, it can be divided into plus pre-bulging and minus pre-bulging [23]. The plus pre-bulging

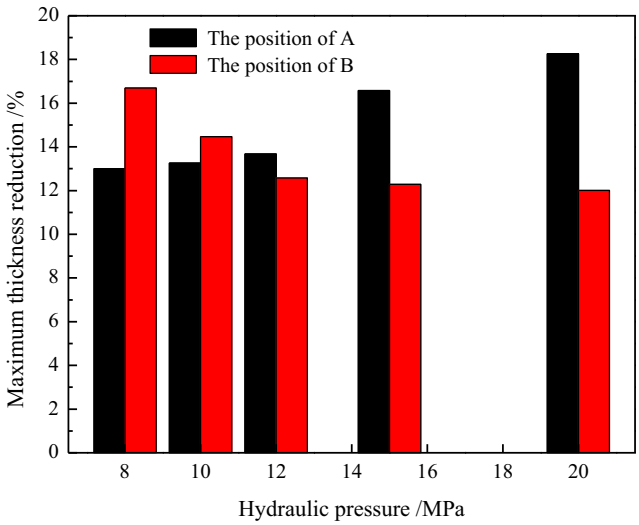

Fig. 18 Maximum wall thickness reduction at position A and B under different hydraulic pressures

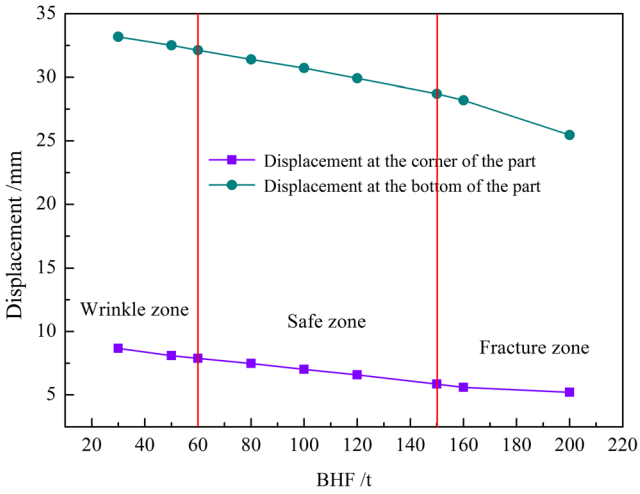

Fig. 19 Rigid-flexible coupling forming window of BHF

fixes the punch at a certain position on the blank before forming (the blank position is the zero position). Then, the loaded hydraulic pressure makes the blank deform inversely to contact the punch, the materials thin out in advance with the increase of stiffness. The minus pre-bulging makes the punch continue to descend at a certain position after touching the blank, and then the hydraulic pressure is loaded, which will let the blank possess more inflows before forming. As shown in Fig. 11, when the plus pre-bulging is used (the loading path 1 in the Fig. 9), the specimen has the phenomenon of multiple wrinkles or even fracture. The reason is that the part has the complex multiple features and the hydraulic pressure is loaded too early in the plus pre-bulging. This makes it difficult to control the blank forming and synchronous and sequential deforming may not be monitored correctly. Meanwhile, the fracture defect would be produced under the extruding of the punch after the wrinkling of the side-wall unconnected region of the specimen corners and the partial local features. The wall thickness distributions of the specimen under the four kinds of

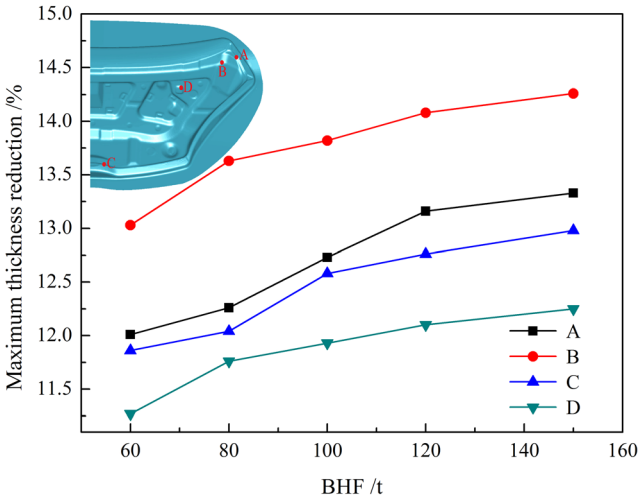

Fig. 20 Wall thickness reductions in points A, B, C, and D with different BHFs

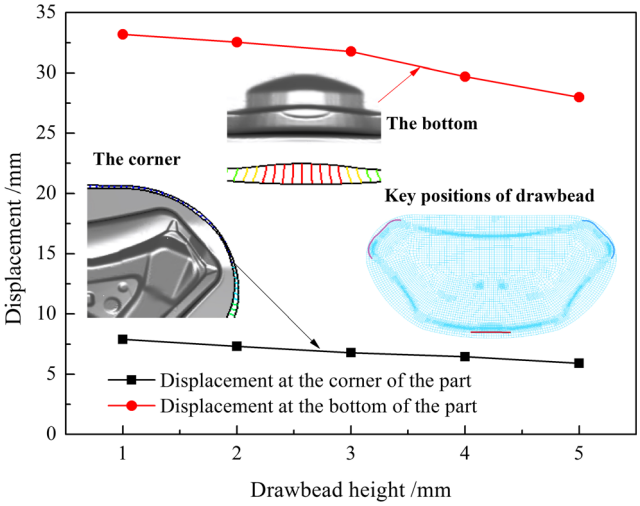

Fig. 21 Blank inflow displacements in the corner and bottom of the specimen under different draw bead heights

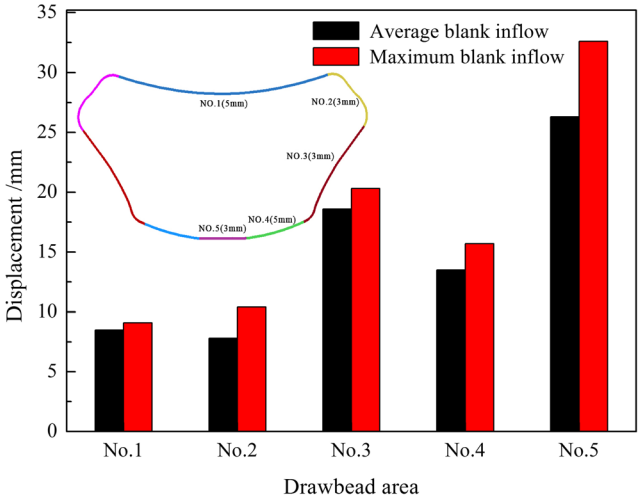

Fig. 23 Average and maximum blank inflow values with optimal parameters of draw bead

loading paths are shown in Fig. 12. In addition, the unevenness level of wall thickness is introduced for further study on the pre-bulging effect, which is defined as:

$$\gamma = \frac{t_{\max} - t_{\min}}{t_0} \times 100\% \tag{27}$$

where $t_{\max}$ is the maximum wall thickness, and $t_{\min}$ is the minimum wall thickness. The variation of γ is depicted in Fig. 13.

As seen in the Fig. 12 and Fig. 13, the wall thickness distribution uniformity and formability of the specimen are the best in the loading path 4. Under the condition of minus pre-bulging and low hydraulic pressure at the initial stage, the material has more inflows into the die cavity. After that, the higher hydraulic pressure is loaded, which makes full use of the friction conservation effect of the hydroforming and be beneficial for the specimen forming. For this kind of

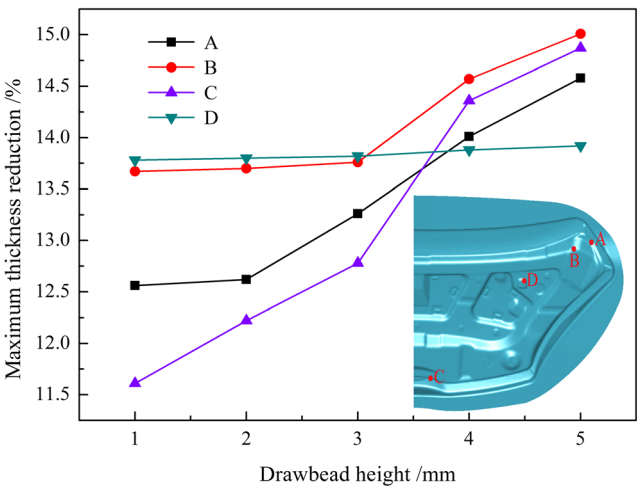

Fig. 22 Wall thickness reductions in points A, B, C, and D under different draw bead heights

specimen, the hydraulic pressure does not need to be loaded too early during the forming process, like the path 2. It will cause the material to stick to the small features of the punch in advance, so that its surrounding blank cannot flow smoothly, and the excessive thinning occurs at the tip.

The maximum hydraulic pressure also plays a significant role at the rigid-flexible coupling stage of the later forming. Five loading paths are designed, as depicted in Fig. 14, with maximum hydraulic pressures varying from 8 to 20 MPa. The punch fitting processes of the typical position A and B of the specimen under different hydraulic pressure conditions are shown in Fig. 15. As seen in the figure, when the hydraulic pressure is low at the rigid-flexible coupling stage of the later forming, the enough friction conservation effect cannot be formed at the position A, resulting in serious thinning and even fracture. Its meridional tensile stress is too large and the deformation is close to the plane strain state. However, for the position B, although the low hydraulic pressure makes the materials hard to entirely fit the punch at the initial stage of the rigid-flexible coupling forming, the blank finally fits the punch properly under the coupling effect of the local rigid insert block and the low hydraulic pressure. The specimen formed by using the maximum hydraulic pressure of 8 MPa is shown in Fig. 16, which indicates that the fracture has appeared at the position A. When the hydraulic pressure is large at the rigid-flexible coupling stage of the later forming, the friction conservation effect of position A is good with high forming quality. However, under the large hydraulic pressure, the rounded corner at the position B constantly is filled and the surrounding material cannot flow. The rounded corner can only be formed by blank self-thinning, which eventually will thin seriously and even fracture. It may lead to failure to form the rigid-flexible effect. Its meridional and zonal tensile stresses are large. The specimen formed by using the maximum hydraulic pressure of 20 MPa is shown in Fig. 17, which indicates that the fracture has appeared at the position B. The

(a) The supplementary part (b) The final part

Fig. 24 Qualified part manufactured by using the proposed rigid-flexible coupling forming process. **a** The supplementary part. **b** The final part

maximum wall thickness reductions at positions A and B under different hydraulic pressures are shown in Fig. 18. Analysis of synthesis exhibits that the specimen forming quality is the best when the maximum hydraulic pressure is 12 MPa.

5.2 Influence of BHF on the inflow of blank

For the rigid-flexible coupling forming of the automobile inner panel, the blank holder force (BHF) must be in the reasonable range, from the critical BHF of wrinkling to the critical BHF of fracture. The region consisting of all the reasonable BHFs is called the forming window, which represents the formability of aluminum alloy sheet and is an important basis for determining the forming process. The forming window of BHF obtained by rigid-flexible coupling tests for the aluminum alloy inner panel is shown in Fig. 19, which provides the critical BHF when the blank is in wrinkle and fracture conditions. As seen in the figure, the specimen gets wrinkled when the BHF is less than 60 t and it ruptures when the BHF is more than 150 t, so the safety ranges of BHFs during forming are from 60 to 150 t. Meanwhile, with the increase in the BHF, the blank inflow values in the corner and bottom of the specimen (the position is shown in Fig. 21) decrease gradually. Due to the different shapes of the local features, the whole blank inflow values in the bottom are higher than that in the corner. The wall thickness reductions in points A, B, C, and D on the surface of the specimen corresponding to the BHF changes are shown in Fig. 20, exhibited definitely different under the same BHF. The reduction of point D is the best but point B has the inferior reduction among all points. Due to the long distance from the specimen edge, the sensibility of point D to the BHF value is inferior to the other 3 points. However, for the point B, the material inflow value is small because of the huge bending before the materials inflow and large depth and deformation of the specimen. With the increase in the BHF, the value of the material to the die cavity decreases while the specimen thickness reduction increases clearly.

5.3 Influence of draw bead on the inflow of blank

The influence of the draw bead height on the blank inflow value is investigated by setting the draw bead heights as 1, 2, 3, 4, and 5 mm, respectively. The blank inflow displacements in the corner and bottom of the specimen corresponding to the changes of draw bead height are shown in Fig. 21. It can be seen that with the increase in the draw bead height, the blank inflow value of the specimen decreases. In addition, the reduced amplitude of the blank inflow value in the bottom is obviously larger than that in the corner. The wall thickness reductions in points A, B, C, and D on the surface of the specimen under different draw bead heights are shown in Fig. 22. With the increase in the draw bead height, the wall thickness reductions of the three typical positions (points A, B, and C) have the tendency to increase obviously, but the reduction of point D is not obvious because of the long distance from the specimen edge. Therefore, the reasonable application of the draw bead can control the flow of material effectively during the rigid-flexible coupling forming of the aluminum alloy automobile body panel. The different draw bead heights are selected comprehensively according to the blank inflow values and the wall thickness reductions of different positions in the specimen. Its average and maximum blank inflow values are shown in Fig. 23. This parameter of the draw bead can satisfy the forming requirement of the specimen well and also is able to be beneficial to the decrease of springback.

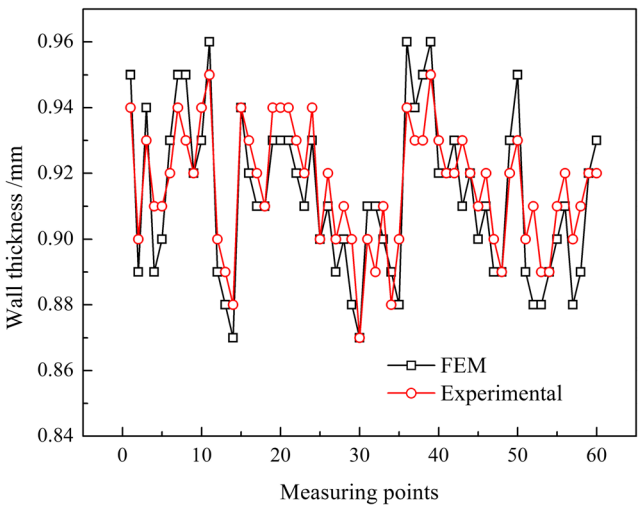

Fig. 25 Comparison of thickness distributions between FEM and experiment

The qualified specimen manufactured by using the proposed rigid-flexible coupling forming process is shown in Fig. 24. The wall thickness was measured by the ultrasonic thickness gauge and compared with the result of FEM, as depicted in Fig. 25. The results of the test coincide well with FEM. Meanwhile, it also indicated that the rigid-flexible coupling forming process can be well used for manufacturing this kind of complex multi-feature sheet parts.

6 Conclusions

(1) In order to achieve the precision forming for the complex multi-feature/small-feature aluminum alloy sheet parts, the rigid-flexible coupling forming process is proposed in this paper, which is a new derivative technique combing the hydroforming and rigid forming in a single stage, having both forming advantages. In addition, it would also broaden the complexity and functional requirement of the parts formed by hydroforming.

(2) The relationship between the local rounded corner feature and the hydraulic pressure is given by theoretical calculation, which provides the theoretical basis for the design of the hydraulic pressure loading path.

(3) For the complex aluminum alloy inner panel of automobile engine hood researched in this paper, the optimal maximum hydraulic pressure is 12 MPa. The hydraulic pressure does not need to be loaded too early during the forming process, like the path 2. In fact, it will cause the material wrinkling and also stick to the small features of the punch in advance, so that its surrounding blank cannot flow smoothly, and the excessive thinning even fracture occurs at the tip.

(4) The forming window of BHF is obtained by the rigid-flexible coupling test for the aluminum alloy inner panel. With the increase in the BHF, the material's inflow to the die cavity decreases while the specimen thickness reduction increases clearly. The reasonable parameters of the draw bead can satisfy the forming requirement of the specimen well and also is able to be beneficial to the decrease of springback. With the increase in the draw bead height, the restriction effect of the materials flow increases obviously.

Acknowledgments The authors gratefully acknowledge the financial support from National Science and Technology Major Project of China with Grant No.2014ZX04002041.

References

1. Schöggl JP, Baumgartner RJ, Hofer D (2016) Improving sustainability performance in early phases of product design: a checklist for sustainable product development tested in the automotive industry. J Clean Prod 140:1602–1617
2. Moon SK, ET Y, Hwang J, Yoon YJ (2014) Application of 3D printing technology for designing light-weight unmanned aerial vehicle wing structures. Int J Precis Eng Manuf-Green Technol 1(3):223–228. https://doi.org/10.1007/s40684-014-0028-x
3. Saxena KK, Drotleff K, Mukhopadhyay J (2016) Elevated temperature forming limit strain diagrams of automotive alloys Al6014-T4 and DP600: a case study. J Strain Anal Eng Des 51(6):459–470. https://doi.org/10.1177/0309324716651028
4. Hörhold R, Müller M, Merklein M, Meschut G (2016) Mechanical properties of an innovative shear-clinching technology for ultra-high-strength steel and aluminium in lightweight car body structures. Weld World 6:613–620
5. Wang ZJ, Zheng LH, Liu ZG, Xiang N, Wang PY (2016) Investigation of viscous pressure forming for 6K21-T4 aluminum alloy car panels. Int J Adv Manuf Technol 85(9-12):2525–2534. https://doi.org/10.1007/s00170-015-8018-x
6. Choi W, Yeo HT, Park JH, GH O, Park SW (2007) A study on press forming of automotive dub-frame parts using extruded aluminum profile. J Mater Process Technol 180:85–88
7. Jeon YJ, Song MJ, Kim HK, Cha BS (2015) Effect of hot-stamping process conditions on the changes in material strength. Int J Automot Technol 16(4):619–627. https://doi.org/10.1007/s12239-015-0063-9
8. Zeng ZP, Zhang YS, Zhou Y, Jin QL (2005) Superplastic forming of aluminum alloy car body panels. Mater Sci Forum 475-479: 3025–3028. https://doi.org/10.4028/www.scientific.net/MSF.475-479.3025
9. Wang Z, Li Y (2008) Formability of 6k21-T4 car panel sheet for viscoelastic–plastic flexible-die forming. J Mater Process Technol 201(1-3):408–412. https://doi.org/10.1016/j.jmatprotec.2007.11.301
10. Lang LH, Wang YM, Xie YS, Yang XY, YQ X (2012) Pre-bulging effect during sheet hydroforming process of aluminum alloy box with unequal height and flat bottom. Trans Nonferrous Met Soc China 22:302–308
11. Djavanroodi F, Abbasnejad DS, Nezami EH (2011) Deep drawing of aluminum alloys using a novel hydroforming tooling. Mater Manuf Process 26(5):796–801. https://doi.org/10.1080/10426911003720722
12. Abedrabbo N, Zampaloni MA, Pourboghrat F (2005) Wrinkling control in aluminum sheet hydroforming. Int J Mech Sci 47(3): 333–358. https://doi.org/10.1016/j.ijmecsci.2005.02.003
13. Brooke L (1997) Hydroforming hits the big time. Automot Ind 177: 57–61
14. Zhang R, Lang L, Zafar R, Lin L, Zhang W (2016) Investigation into thinning and spring back of multilayer metal forming using hydro-mechanical deep drawing (HMDD) for lightweight parts. Int J Adv Manuf Technol 82(5-8):817–826. https://doi.org/10.1007/s00170-015-7415-5
15. Hu H, Wang JF, Fan KT, Chen TY, Wang SY (2015) Development of sheet hydroforming for making an automobile fuel tank. P I Mech Eng B-J Eng 229:654–663
16. Palumbo G (2013) Hydroforming a small scale aluminum automotive component using a layered die. Mater Des 44:365–373. https://doi.org/10.1016/j.matdes.2012.08.013
17. Liu XJ, Liu CH, Wang X, Wan SX, Fu JR (2016) Numerical simulation study on divided region variable blank holder force of automobile outdoor in hydrodynamic deep drawing. Hot Work Technol 45:146–149
18. Modi B, Kumar DR (2013) Effect of friction and lubrication on formability of AA5182 alloy in hydroforming of square cups. Mater Sci Forum 762:621–626. https://doi.org/10.4028/www.scientific.net/MSF.762.621

19. Abdelkefi A, Malécot P, Boudeau N, Guermazi N, Haddar N (2016) Evaluation of the friction coefficient in tube hydroforming with the "corner filling test" in a square section die. Int J Adv Manuf Technol 88:2265–2273
20. Lang LH (2014) Innovative sheet hydroforming and warm/hot hydroforming. National Defense Industry Press, Beijing
21. Kong DS, Lang LH, Sun ZY, Ruan SW, SS G (2016) A technology to improve the formability of thin-walled aluminum alloy corrugated sheet components using hydroforming. Int J Adv Manuf Technol 84(1-4):737–748. https://doi.org/10.1007/s00170-015-7727-5
22. Choi H, Koc M, Ni J (2007) A study on the analytical modeling for warm hydro-mechanical deep drawing of lightweight materials. Int J Mach Tools Manuf 47(11):1752–1766. https://doi.org/10.1016/j.ijmachtools.2006.12.005
23. Meng B, Wan M, Yuan S, XD X, Liu J, Huang ZB (2013) Influence of cavity pressure on hydrodynamic deep drawing of aluminum alloy rectangular box with wide flange. Int J Mech Sci 77:217–226. https://doi.org/10.1016/j.ijmecsci.2013.10.012